Available online at www.sciencedirect.com
SCIENCE DIRECT®
Journal of Solid State Chemistry 172 (2003) 431–437
JOURNAL OF SOLID STATE CHEMISTRY
http://elsevier.com/locate/jssc

Rigid unit modes (RUMs) of distortion, local crystal chemistry and the inherent displacive flexibility of microporous $AlPO_4$-11

Yun Liu and Ray L. Withers*

Research School of Chemistry, Australian National University, Canberra, ACT 0200, Australia

Received 7 October 2002; accepted 9 December 2002

Abstract

Electron diffraction is used to investigate the average structure of microporous $AlPO_4$-11 as well as the zero-frequency rigid unit mode (RUM) modes of distortion of the ideal $AlPO_4$-11 tetrahedral framework. Direct experimental evidence (in the form of a highly structured, characteristic diffuse intensity distribution) has been found for the (presumably dynamic) excitation of numerous zero-frequency RUM modes of distortion. The lattice dynamic program CRUSH is used to confirm the existence of zero-frequency RUM modes of distortion with wave-vectors falling on the observed diffuse distribution. The simultaneous (presumably dynamic) excitation of such RUM modes of distortion needs to be taken into account in order for the local crystal chemistry of $AlPO_4$-11 to be understood.

Keywords: Microporous $AlPO_4$-11; Characteristic diffuse distribution; Dynamical disorder; Correlated tetrahedral rotation

1. Introduction

The $AlPO_4$ family of molecular sieve materials was first discovered in the early 1980s [1]. They have since been studied extensively, particularly the metal ion-substituted derivatives thereof, as a result of their ion exchange and catalysis properties [2–6]. The topological connectedness of the constituent $(Al,P)O_4$ tetrahedra for the 11th member of this series, $AlPO_4$-11, was first predicted by Bennett and Smith [7] from X-ray determined, body-centred cell dimensions ($a \sim 13.5$, $b \sim 18.7$, $c \sim 8.45$ Å) as was the highest possible space group symmetry compatible with this topological connectedness (*Icmm* if Al/P ordering is ignored, *Icm*2 if Al/P ordering is taken into account—see Fig. 1).

Neutron Rietveld refinements of calcined $AlPO_4$-11 [8,9] (unfortunately only powder specimens of pure $AlPO_4$-11 are to date available) have since been carried out in both space group symmetries and confirmed the predicted topological connectedness of the tetrahedral framework (as has a rather more detailed single-crystal structure refinement in space group *Icm*2 of a closely related Mn-doped, organic template encapsulated $(MnAl_9)P_{10}O_{40} \cdot C_6H_{16}N$, MnAPO-11 analogue phase [10]). The authors of these papers, however, also pointed out several suggestive problems associated with the refinement process and resultant refined structures. In particular, attention was drawn to "…a significant non-crystalline contribution to the total scattering,…as evidenced by an additional slowly oscillating component superimposed on the Bragg pattern…" [8,9]. The justification for the removal of this non-crystalline scattering was the assumption that it was due to a distinct "…amorphous phase" [8,9] and not unavoidably associated with "crystalline" $AlPO_4$-11 itself. The extracted interatomic correlation distances associated with this "non-crystalline" scattering, however, were all very close to those characteristic of crystalline $AlPO_4$-11 [9] suggesting the "…amorphous phase" assumption may well not be justified.

Recent total scattering studies of closely related materials, SiO_2-tridymite in particular [11], have shown that the co-existence of an oscillating diffuse background and relatively sharp Bragg reflections is quite common for tetrahedral framework structures of this sort [11,12]. The Bragg peaks, in such cases, provide information on the time-averaged crystal structure while

*Corresponding author. Fax: +61-26-125-0750.
E-mail address: withers@rsc.anu.edu.au (R.L. Withers).

0022-4596/03/$ - see front matter © 2003 Elsevier Science (USA). All rights reserved.
doi:10.1016/S0022-4596(03)00024-0

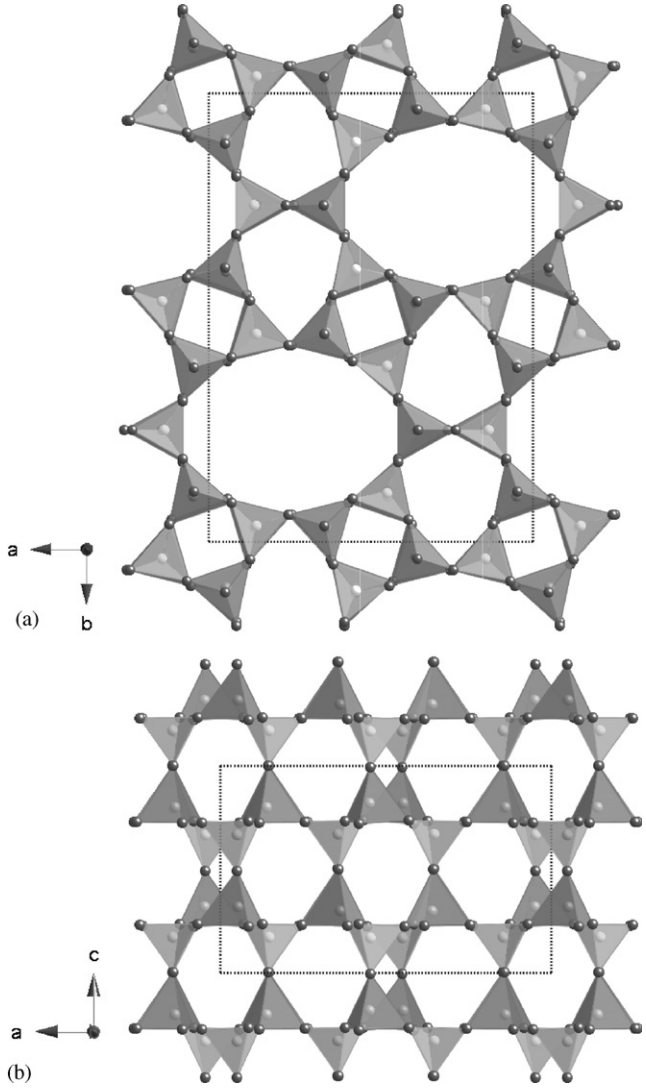

Fig. 1. The *Icm*2, $AlPO_4$-11 type, corner-connected, tetrahedral framework of MnAPO-11 (*10*) is shown in projection down the [001] direction in (a) and along the orthogonal [010] direction in (b). The larger $(Al_{0.9}Mn_{0.1})O_4$ tetrahedra are darker while the smaller PO_4 tetrahedra are lighter.

the background diffuse scattering provides information on the instantaneous local structure. While the time-averaged structure in such cases is sufficient to obtain the appropriate topological connectedness of the constituent tetrahedra, instantaneous local crystal structure is also needed if the local crystal chemistry (tetrahedral sizes, T–O–T bond angles, etc.) is to make sense. In addition to structured diffuse scattering [13–16], orientationally disordered systems of this sort tend to be characterized by average structures with short T–O bond distances within constituent TO_4 tetrahedra (see, for example, Fig. 7 of [11]), relatively poor local crystal chemistry as judged, for example, by bond valence sum calculations [17] and by large and/or strongly anisotropic temperature factors [11,12].

Just such sorts of crystal chemical problems (short Al–O and P–O bond distances, wide spreads in Al–O–P bond angles, close to 180° Al–O–P bond angles, relatively poor local crystal chemistry, large and/or strongly anisotropic temperature factors, etc.) are characteristic of the refined average structures of $AlPO_4$-11 [8–10] reported to date (see Tables 1 and 2). Table 2, for example, shows bond valence sums or apparent valences (AVs) [17] calculated using the *Icm*2 refinements of [9] and [10], respectively. While the local crystal chemistry of the average tetrahedral framework structure determined from the single-crystal structure refinement of MnAPO-11 [10] appears to be significantly improved over that determined from neutron Rietveld refinement of $AlPO_4$-11 [9] (despite the difficulties in interpretation associated with the presence of an encapsulated organic species and the substitution of 10% of the Al ions by Mn ions in the former case), a large number of ions remain quite significantly over-bonded in both cases. It is also noteworthy that it is the most over-bonded O ions that are also associated with the largest and most strongly anisotropic temperature factors in the case of MnAPO-11 [10]. This suggests that relatively large amplitude, correlated tetrahedral rotation modes, rigid unit mode (RUM) modes, may well be dynamically excited in $AlPO_4$-11, even at room temperature [11–16].

Thus the prime purpose of the current paper is to present the results of an electron diffraction search for the structured diffuse scattering characteristic of such an orientationally flexible framework structure and which map out the zero-frequency RUM modes of distortion of $AlPO_4$-11. The lattice dynamical program CRUSH [18] is used to interpret the observed diffuse scattering.

2. Experimental

2.1. Synthesis

The $AlPO_4$-11 precursor was prepared by a sol–gel process. The reaction mixture was prepared by slowly dropping a mixture of orthophosphoric acid (H_3PO_4, 85 wt%, Univar; 2.729 mL) and H_2O (2 mL) into a solution composed of boehmite alumina (Al_2O_3, 75 wt%, HiQ-30, Alcoa; 2.720 g) and H_2O (7.40 mL). The resultant viscous solution was manually stirred until homogenization, and then aged at room temperature for 2 h with periodic stirring at intervals of 20 min. A mixture of di-*n*-propylamine (Pr_2NH:$(C_3H_7)_2NH$, 99%, Aldrich; 2.77 mL) and H_2O (5.0 mL) was then slowly added into the above aged solution. The resultant solution was then subjected to thorough stirring and aging for 2 h at room temperature to form a uniform gel. The gel composition in molar ratios was: Pr_2NH:

Table 1
Selected bond distances (T–O) and angles (T–O–T) for $AlPO_4$-11 calculated from the average structure refinements reported in [9,10] in space groups *Icm*2 [9,10] and *Icmm* [9]

Bond angle (°)	*Icm*2 [9]	*Icm*2 [10]	Bond angle (°)	*Icmm* [9]	Bond angle (°)	$P3_121$ [11]
	$a=13.5336$ Å $b=18.4821$ Å $c=8.3703$ Å	$a=13.472$ Å $b=18.712$ Å $c=8.4431$ Å		$a=13.5333$ Å b = 18.4845 Å $c=8.3703$ Å		$a=4.9423$ Å $b=4.9423$ Å $c=10.9446$ Å
P(1)–O(1)–Al(1)	167	178	T(1)–O(1)–T(1)	151	P(1)–O(1)–Al(1)	143
P(2)–O(2)–Al(2)	174	174	T(2)–O(2)–T(2)	165	P(1)–O(2)–Al(1)	142
P(3)–O(3)–Al(3)	172	175	T(3)–O(3)–T(3)	177		
P(1)–O(4)–Al(1)	131	144	T(1)–O(4)–T(1)	127		
P(1)–O(5)–Al(2)	140	151	T(1)–O(5)–T(2)	144		
P(2)–O(5′)–Al(1)	147	144	T(1)–O(6)–T(2)	149		
P(1)–O(6)–Al(2)	152	154	T(2)–O(7)–T(3)	172		
P(2)–O(6′)–Al(1)	140	153	T(3)–O(8)–T(3)	180		
P(3)–O(7)–Al(2)	166	165				
P(2)–O(7′)–Al(3)	168	168				
P(3)–O(8)–Al(3)	175	177				
Bond distance (Å)			Bond distance (Å)		Bond distance (Å)	
Al(1)–O(1)	1.64	1.720	T(1)–O(1)	1.67	Al(1)–O(1)	1.731
Al(1)–O(4)	1.84	1.743	T(1)–O(4)	1.80	Al(1)–O(1)	1.732
Al(1)–O(5′)	1.58	1.752	T(1)–O(5)	1.62	Al(1)–O(2)	1.739
Al(1)–O(6′)	1.60	1.702	T(1)–O(6)	1.45	Al(1)–O(2)	1.739
Mean	1.67	1.729	Mean	1.64	Mean	1.735
Al(2)–O(2)	1.68	1.667	T(2)–O(2)	1.57		
Al(2)–O(5)	1.74	1.718	T(2)–O(5)	1.58		
Al(2)–O(6)	1.54	1.696	T(2)–O(6)	1.57		
Al(2)–O(7)	1.67	1.683	T(2)–O(7)	1.52		
Mean	1.66	1.691	Mean	1.56		
Al(3)–O(3)	1.80	1.767	T(3)–O(3)	1.63		
Al(3)–O(7′)	1.69	1.643	T(3)–O(7)	1.64		
Al(3)–O(7′)	1.69	1.643	T(3)–O(7)	1.64		
Al(3)–O(8)	1.63	1.688	T(3)–O(8)	1.49		
Mean	1.70	1.685	Mean	1.60		
P(1)–O(1)	1.57	1.438			P(1)–O(1)	1.522
P(1)–O(4)	1.66	1.493			P(1)–O(1)	1.523
P(1)–O(5)	1.64	1.510			P(1)–O(2)	1.521
P(1)–O(6)	1.39	1.531			P(1)–O(2)	1.520
Mean	1.57	1.493			Mean	1.522
P(2)–O(2)	1.50	1.481				
P(2)–O(5′)	1.48	1.506				
P(2)–O(6′)	1.56	1.501				
P(2)–O(7′)	1.52	1.503				
Mean	1.52	1.498				
P(3)–O(3)	1.31	1.364				
P(3)–O(7)	1.57	1.491				
P(3)–O(7)	1.57	1.491				
P(3)–O(8)	1.35	1.454				
Mean	1.45	1.450				
⟨T–O⟩	1.595	1.591		1.60		1.629

For comparison purposes, the equivalent bond distances and angles are also given for the low quartz form of berlinite, space group $P3_121$.

Al_2O_3:P_2O_5:$40H_2O$. This gel was poured into a small Teflon cup supported by a Teflon holder, which was then placed in a Teflon-lined stainless-steel pressure vessel. 100 mL of external water was kept at the bottom of the vessel to increase the steam pressure of the hydrothermal reaction, in such a manner that the gel in the cup never came into direct contact with the external water. The gel and water were then sealed and heated in an oven at 200°C for 24 h. The vessel was then taken out from the oven and quenched in water.

Table 2
Bond valence sums or AVs calculated from the *Icm*2 average structure refinements reported in [9,10]

Structure	*Icm*2 [9]	*Icm*2 [4]	Ideal
Bond valence parameter R	Al–O = 1.651 Å P–O = 1.604 Å O–O = 1.480 Å	Al–O = 1.651 Å P–O = 1.604 Å O–O = 1.480 Å	Al–O = 1.7574 Å P–O = 1.5214 Å O–O = 2.4844 or 2.8698 Å
At Al(1)	**4.009**	3.241	3.000
At Al(2)	**4.005**	**3.603**	
At Al(3)	**3.491**	**3.690**	
At P(1)	4.689	5.412	5.000
At P(2)	5.189	5.338	
At P(3)	**6.204**	**6.105**	
At O(1)	2.118	**2.414**	2.000
At O(2)	2.312	**2.359**	
At O(3)	**2.752**	**2.608**	
At O(4)	**1.492**	2.122	
At O(5)	1.709	2.122	
At O(5′)	**2.702**	2.056	
At O(6)	**3.004**	2.101	
At O(6′)	2.328	2.188	
At O(7)	2.075	2.283	
At O(7′)	2.142	2.338	
At O(8)	2.964	**2.409**	

($V = \exp((R-d)/0.37\,\text{Å})$, calculated using the bond valence parameters listed in [17]). Sites where the calculated AV deviates markedly from the expected ideal AV are highlighted in bold.

The as-synthesized solid product was recovered by filtration, washed with distilled water and acetone, and dried in air at 50°C. Samples calcined in air were obtained after heat treatment, respectively, at 200°C, 400°C and 600°C for 24 h.

2.2. X-ray powder diffraction

The average structure unit-cell dimensions of the resultant samples were refined using a least-squares program from data collected with a Guinier–Hägg camera. Silicon ($a = 5.4310280$ Å at 22.5°C) was used as an internal standard.

2.3. Electron diffraction

Crushed specimens were deposited on holey-carbon coated grids and examined in a Philips EM 430 Transmission Electron Microscope. Given the sensitivity of the specimens to electron beam irradiation, electron dose was always minimized as far as possible.

3. Results

3.1. Powder XRD

The average structure cell dimensions of the as-prepared $AlPO_4$-11 phase were determined to be orthorhombic (*Icm*2), $a = 13.352(3)$ Å, $b = 18.668(4)$ Å, and $c = 8.4407(18)$ Å, in good agreement with previously published results [7,19]. This specimen was quite stable at room temperature with the cell dimensions after 65 days changing by less than 0.1%. Heating in air, at temperatures as low as 200°C, led to the rapid physisorption of water and a structural change from *Icm*2 to $Pbn2_1$ ($a = 13.851(3)$ Å, $b = 18.004(3)$ Å, and $c = 8.1255(17)$ Å). Heating in air at higher temperatures led to no further changes.

3.2. Electron diffraction

Crushed crystal fragments of the as-prepared $AlPO_4$-11 phase almost invariably had a plate-like morphology with the plate normal corresponding to the crystallographic **b**-axis so that by far the most commonly obtained major zone axis orientation observed was [010]. Fig. 2a, for example, shows a typical [010] zone axis electron diffraction pattern (EDP). The measured c/a ratio from such patterns was always found to be ~2% smaller than that of the as-prepared $AlPO_4$-11 phase determined by XRD, but consistent with the cell dimensions reported for calcined dry $AlPO_4$-11 by Richardson et al. [9]. Very occasionally, [001] zone axis EDPs were also obtained as shown in Fig. 2b. The measured a/b ratio from such patterns was this time found to be ~2% larger than that of the as-prepared $AlPO_4$-11 phase, but again consistent with the $a_p = 13.5336$, $b_p = 18.4821$, $c_p = 8.3703$ Å cell dimensions reported for calcined dry $AlPO_4$-11 by Richardson et al. [9]. We thus believe that any physisorbed water or remaining organic template in the as-prepared $AlPO_4$-11

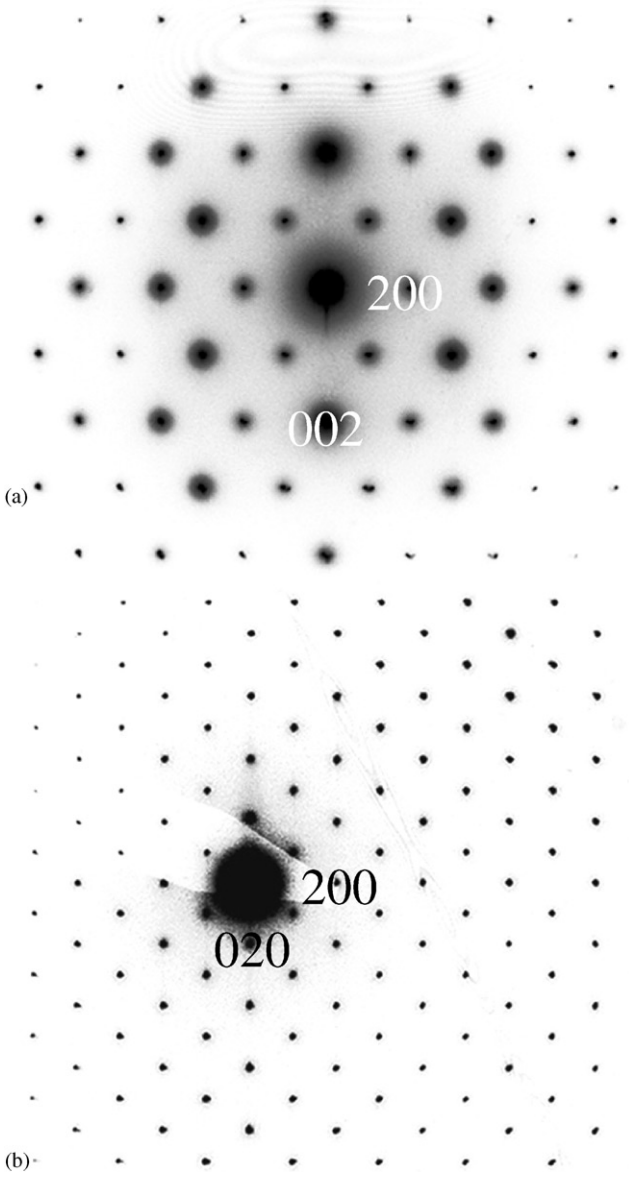

Fig. 2. Typical (a) [010] and (b) [001] zone axis EDPs of $AlPO_4$-11.

phase is removed either via the high vacuum in the TEM column and/or under the electron beam so that the material investigated in the TEM corresponds to calcined dry $AlPO_4$-11.

[100] zone axis orientations, however, were never obtained so that the *c* glide perpendicular to **a** of the expected *Icm*2 average structure could not be confirmed by electron diffraction. What could be unequivocally confirmed, however, was the absence of any additional satellite reflections in addition to the strong Bragg reflections expected for an underlying *Icm*2 parent structure. This rules out both the *P*2 energy minimized structures for $AlPO_4$-11 proposed on theoretical grounds in [20,21] as well as all proposed unit cells and space group symmetries necessitating a

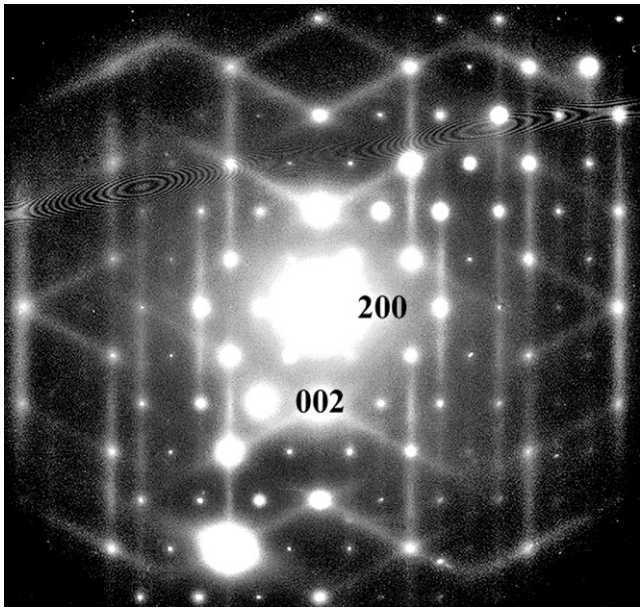

Fig. 3. A typical, close to [010] zone axis EDP of $AlPO_4$-11 showing the presence of strong and quite sharp diffuse streaking running along the $\langle 301 \rangle^*$ as well as $[001]^*$ directions of reciprocal space. This characteristic diffuse streaking disappears at the exact zone axis orientation (cf. Fig. 3 with Fig. 2a).

superstructure expansion of the parent a_p, b_p, c_p unit cell.

While no electron diffraction evidence could be found that was incompatible with the expected *Icm*2 average crystal structure, direct electron diffraction evidence was found for the existence of a multitude of zero-frequency RUM modes of distortion of the underlying parent structure in the form of a highly structured, characteristic diffuse intensity distribution. Fig. 3, for example, shows a typical (and quite reproducible) very close to [010] zone axis EDP showing the presence of strong and quite sharp (transverse polarized) diffuse streaking running along the $\langle 301 \rangle^*$ as well as $[001]^*$ directions of reciprocal space. Intriguingly this characteristic diffuse streaking disappears at the exact zone axis orientation (cf. Fig. 3 with Fig. 2a). That this characteristic (in general curved) diffuse intensity distribution is not localized to the vicinity of the [010] zone axis orientation but is an essentially continuous function of reciprocal space is apparent from the (a) $\langle 110 \rangle$ and (b) $\sim \langle 130 \rangle$ zone axis EDPs shown in Fig. 4. Note that it is sometimes possible for what appear to be superlattice peaks to arise when diffuse curves intersect as, for example, occurs in the case of the diffuse blobs at the $[3,1,2l+1]^*$ reciprocal lattice positions in Fig. 4b. Tilting experiments, however, show that there are never sharp Bragg reflections at these positions in reciprocal space.

The presence of this highly structured diffuse intensity distribution is absolutely characteristic of the reciprocal lattice of $AlPO_4$-11 and quite reproducible although

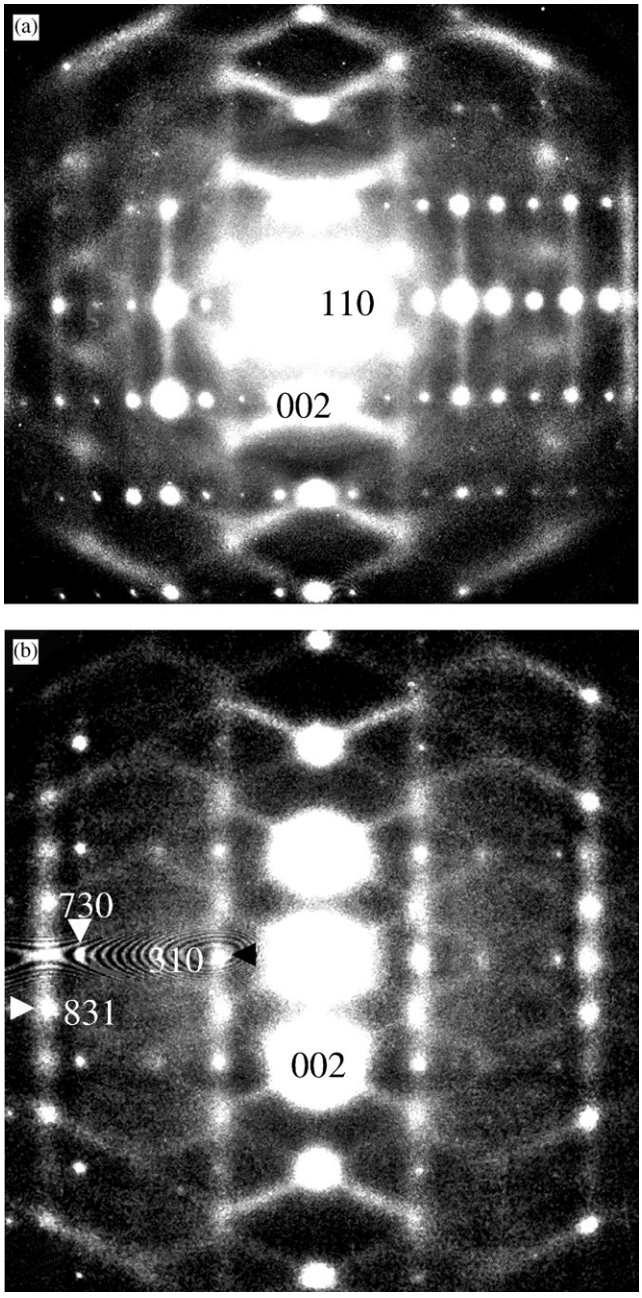

Fig. 4. (a) ⟨110⟩ and (b) ~⟨130⟩ zone axis EDPs of $AlPO_4$-11. Note that it is sometimes possible for what appear to be superlattice peaks to arise when diffuse curves intersect as, for example, occurs in the case of the diffuse blobs at the $[3,1,2l+1]^*$ reciprocal lattice positions in (b). Note also the characteristic curved diffuse scattering in (a) and (b).

difficult to record as a result of the sensitivity of the material to electron beam irradiation. This beam sensitivity in conjunction with the natural crystal morphology of the crushed crystalline flakes makes it difficult to systematically explore the whole of reciprocal space and hence the detailed shape of the observed diffuse distribution. There is, however, no doubt that $AlPO_4$-11 exhibits an extremely characteristic and highly structured diffuse intensity distribution which we believe is equivalent to the "…significant non-crystalline contribution to the total scattering…" observed in powder neutron patterns [8, 9].

Table 3
Fractional coordinates and unit-cell dimensions for idealized *Icmm* $AlPO_4$-11

Unit cell	Label	Site (occupancy)	Fractional coordinates		
	T1	P/Al (0.5/0.5)	0.1448	0.0343	0.1875
$a = 13.8486$ Å	T2	P/Al (0.5/0.5)	0.9510	0.1039	0.3125
$b = 19.2462$ Å	T3	P/Al (0.5/0.5)	0.8616	0.2500	0.1875
$c = 8.7435$ Å	O1	O (1.0)	0.1448	0.0343	0.0000
	O2	O (1.0)	0.9510	0.1039	0.5000
$\alpha = 90°$	O3	O (1.0)	0.8616	0.2500	0.0000
$\beta = 90°$	O4	O (1.0)	0.2500	0.0611	0.2500
$\gamma = 90°$	O5	O (1.0)	0.0599	0.0865	0.2500
	O6	O (1.0)	0.1244	0.9553	0.2500
	O7	O (1.0)	0.9174	0.1805	0.2500
	O8	O (1.0)	0.7500	0.2500	0.2500

4. RUMs of the ideal $AlPO_4$-11 structure type

Given the extreme beam sensitivity of $AlPO_4$-11, it is important to show that the observed structured diffuse scattering is not a result of beam damage but rather an intrinsic, predictable property of the $AlPO_4$-11 tetrahedral framework itself. We have therefore used the lattice dynamics program CRUSH [18] (which gives the lattice dynamical solutions to the equations of motion for a set of linked rigid tetrahedra) to investigate the RUM spectrum of $AlPO_4$-11. Given that both refined *Icm*2 average structures [9,10] are already considerably distorted (see Tables 1 and 2), we have first of all derived an idealized *Icmm* $AlPO_4$-11-type parent structure (see the fractional coordinates and unit-cell dimensions given in Table 3) such that the constituent $(Al,P)O_4$ tetrahedra are each regular and of identical size appropriate to an averaged AlO_4 and PO_4 tetrahedra for the purposes of the CRUSH calculation. (Note that the unit-cell dimensions of this idealized *Icmm* $AlPO_4$-11-type parent structure are each several percent larger than those observed experimentally.) The energies associated with deformation of these individual $(Al,P)O_4$ tetrahedral units is then typically much larger than the energies associated with changes in their relative orientations [11–16] so that only those modes of distortion which entail zero or minimal deformation of these essentially rigid tetrahedral units (RUMs) can reasonably be expected to be thermally excited at room temperature.

Nine RUM modes of distortion, involving purely in-plane rotation axes passing through the basal planes of the tetrahedra, are predicted to exist for any modulation wave-vector of the form $\mathbf{q} = [hk0]^*$. Experimentally, however, diffuse scattering of this form has not been

observed (see, for example, Figs. 3 and 4) suggesting that one or more $\mathbf{q} = \mathbf{0}$ RUM modes of this form may already have condensed out. This would also be consistent with the several percent smaller average structure unit-cell dimensions observed experimentally. Four RUM modes of distortion, also involving in-plane rotation axes but this time coupled with rigid-body shifts are predicted to exist for a general modulation wave-vector of the form $\mathbf{q} = \gamma\mathbf{c}^*$, in agreement with the strong transverse polarized diffuse streaking observed along $\mathbf{c}^*$ experimentally (see Figs. 3 and 4) as well as with the reported anisotropic thermal parameters in [10]. A single RUM mode of distortion is also predicted to exist for modulation wave-vectors running along the $\langle 301 \rangle^*$ direction of reciprocal space, just as is observed experimentally (see Fig. 3). The associated RUM eigenvector, however, is now quite complex and appears to involve tetrahedral rotation around $\mathbf{c}$ as well as in-plane rotation axes. A single zero-frequency RUM mode of distortion is also predicted to exist on the curved (hyperbolic) diffuse distribution apparent in Fig. 4 e.g. close to the $\langle 331 \rangle^*$ direction of reciprocal space in Fig. 4a etc.

We have also repeated the above CRUSH calculations using the unit cell and fractional coordinates determined from the single crystal structure refinement of the MnAPO-11 analogue phase [10] (while this tetrahedral framework is by no means ideal it is rather more regular than the tetrahedral framework refined in [9]). Very similar results were obtained as for the idealized framework structure except that the low-frequency $[hk0]^*$ Q-RUM modes were now not exactly equal to zero frequency and also entailed tetrahedral rotation around $\mathbf{c}$ as well as around in-plane rotation axes. Thus zero-frequency RUM modes of vibration do indeed appear to exist for each point on the experimentally observed diffuse distribution and confirm that the observed diffuse distribution is indeed an intrinsic, predictable property of the $AlPO_4$-11 tetrahedral framework.

Total scattering Rietveld or single crystal structure refinements taking into account this structured diffuse scattering (see, for example, [11,12]) as well as analytical expressions for the RUM modulation wave-vectors and their associated eigenvectors (see, for example, [16]) are now needed in order to obtain a realistic picture of both the inherent displacive flexibility of $AlPO_4$-11 as well as its instantaneous local crystal structure.

5. Conclusions

The inherent displacive flexibility of many zeolites and zeolite-like materials plays an important role in the specificity of many of their physico-chemical properties [6,22,23] and needs to be taken into account in a far more systematic manner than appears to have occurred to date. The fact that the reciprocal lattice of $AlPO_4$-11 is characterized by an intrinsic, highly structured, characteristic diffuse intensity distribution requires the presence of numerous, significantly excited, RUM modes of distortion (whether static or dynamic). It is clearly going to be necessary to consider total scattering refinements (including both Bragg and diffuse scattering) in conjunction with Monte Carlo simulation like those carried out for SiO_2-tridymite, SiO_2-cristobalite and SiO_2-quartz (see, for example, [11,12]) to get a good idea of the instantaneous local structure of $AlPO_4$-11.

References

[1] S.T. Wilson, B.M. Lok, C.A. Messina, T.R. Cannan, E.M. Flanigen, J. Amer. Chem. Soc. 104 (1982) 1146–1147.
[2] E.M. Flanigen, B.M. Lok, R.L. Patton, S.T. Wilson, Pure Appl. Chem. 58 (1986) 1351–1358.
[3] E.M. Flanigen, R.L. Patton, S.T. Wilson, Stud. Surf. Sci. Catal. 37 (1988) 13–27.
[4] D.B. Akolekar, J. Mol. Catal. A: Chemical 104 (1995) 95–102.
[5] D.B. Akolekar, R.F. Howe, J. Chem. Soc., Faraday Trans. 93 (1997) 3263–3268.
[6] P. Demontis, J. Gulín González, G.B. Suffriti, A. Tilocca, C. de las Pozas, Microporous Mesoporous Mater. 42 (2001) 103–111.
[7] J.M. Bennett, J.V. Smith, Z. Kristallogr. 171 (1985) 65–68.
[8] J.M. Bennett, J.W. Richardson, J.J. Pluth, J.V. Smith, Zeolites 7 (1987) 160–162.
[9] J.W. Richardson, J.J. Pluth, J.V. Smith, Acta Crystallogr. B 44 (1988) 367–373.
[10] J.J. Pluth, J.V. Smith, J.W. Richardson, J. Phys. Chem. 92 (1988) 2734–2738.
[11] M.T. Dove, A.K.A. Pryde, D.A. Keen, Miner. Magn. 64 (2000) 267–283.
[12] M.G. Tucker, M.T. Dove, D.A. Keen, Total scattering and reverse Monte Carlo modelling of disordered crystalline materials, in: S.J.L. Billinge, M.F. Thorpe (Eds.), From Semiconductors to Proteins: Beyond the Average Structure, Kluwer Academic, Plenum Publishers, Dordrecht, New York, 2002, pp. 85–103.
[13] R.L. Withers, J.G. Thompson, T.R. Welberry, Phys. Chem. Miner. 16 (1989) 517–523.
[14] R.L. Withers, J.G. Thompson, Y. Xiao, R.J. Kirkpatrick, Phys. Chem. Miner. 21 (1994) 421–433.
[15] M.T. Dove, K.D. Hammonds, V. Heine, R.L. Withers, Y. Xiao, R.J. Kirkpatrick, Phys. Chem. Miner. 23 (1996) 56–62.
[16] R.L. Withers, Y. Tabira, J.A. Valgoma, M. Aroyo, M.T. Dove, Phys. Chem. Miner. 27 (2000) 747–756.
[17] N.E. Brese, M. O'Keeffe, Acta Crystallogr. B 47 (1991) 192–197.
[18] K.D. Hammonds, M.T. Dove, A.P. Giddy, V. Heine, Amer. Miner. 79 (1994) 1207–1209.
[19] N.J. Tapp, N.B. Milestone, M.E. Bowden, R.H. Meinhold, Zeolites 10 (1990) 105–110.
[20] E. de Vos Burchart, H. van Bekkum, B. van de Graaf, E.T.C. Vogt, J. Chem. Soc. Faraday Trans. 88 (1992) 2761–2769.
[21] N.J. Henson, A.K. Cheetham, J.D. Gale, Chem. Mater. 8 (1996) 664–670.
[22] K.D. Hammonds, H. Deng, V. Heine, M.T. Dove, Phys. Rev. Lett. 78 (1997) 3701–3704.
[23] K.D. Hammonds, V. Heine, M.T. Dove, J. Phys. Chem. B 102 (1998) 1759–1767.